Journal of The Electrochemical Society, **152** (1) D1-D5 (2005)
0013-4651/2004/152(1)/D1/5/$7.00 © The Electrochemical Society, Inc.

Displacement Synthesis of Cu Shells Surrounding Co Nanoparticles

Zhanhu Guo,[a,b,*] Challa S. S. R. Kumar,[b] Laurence L. Henry,[c] E. E. Doomes,[b] Josef Hormes,[b] and Elizabeth J. Podlaha[a,,z]**

[a]*Gordon A. and Mary Cain Department of Chemical Engineering, Louisiana State University, Baton Rouge, Louisiana 70803, USA*
[b]*Center for Advanced Microstructures and Devices, Louisiana State University, Baton Rouge, Louisiana 70806, USA*
[c]*Department of Physics, Southern University and A&M College, Baton Rouge, Louisiana 70813, USA*

Copper shells were fabricated by a displacement method around Co nanoparticles (3.2 ± 0.6 nm) at room temperature in a copper-citrate aqueous electrolyte. The nanoparticles were synthesized by a wet chemical approach using the surfactant sulfobetaine, dodecyldimethyl (3-sulfopropyl) ammonium hydroxide (98%) in tetrahydrofuran. X-ray absorption near-edge structure analysis confirmed that cobalt oxide was not present in the nanoparticles upon exposure to air, consistent with a shell formation. Additionally, the presence of the shell resulted in an increase of the blocking temperature of the core-shell nanoparticles, stabilizing the ferromagnetic behavior up to 235 K.
 [DOI: 10.1149/1.1825384]

Manuscript submitted April 6, 2004; revised manuscript received June 1, 2004. Available electronically November 17, 2004.

The iron-group nanoparticles, cobalt,[1-14] iron,[3,15-17] and nickel,[3,17,18] are of interest due to their unusual magnetic properties, such as an enhanced coercivity compared to thin films or microsized particles.[1,19] Platinum alloys of Co and Fe nanoparticles have gained recent attention in high-density data storage, due to their inherent high magnetic anisotropy.[20-30] In addition, nanoparticles have been synthesized with alloys of the iron-group elements themselves, including, *e.g.*, FeCo,[31] CoNi,[32] and CoNiB.[33] A common challenge in all these examples is the control of surface properties, because iron-group nanoparticles readily oxidize in air, which requires that the nanoparticles be stored in a protective air environment, such as N_2. Cobalt oxide formation is not necessarily deleterious if the oxide shell is stabilized. For example, Co nanoparticles embedded and dispersed in a CoO matrix[34] result in an increase in the blocking temperature compared to uncoated Co nanoparticles.

In an effort to control the surface chemistry of nanoparticles, the fabrication of a compact noble shell, such as gold,[35-39] platinum,[40] or silver,[41] around the vulnerable nanoparticle has been demonstrated. The reported methods include a microemulsion technique where the metallic shell ions were reduced with an additional reduction agent[35,36,38] added to the solution containing nanoparticles. Displacement reactions, where part of the cobalt nanoparticle is sacrificed as the reducing agent for the noble metal deposition, have been used for gold and platinum.[37,40] Also, a high-temperature transmetallation reaction (200°C) has been used to form an Au shell around Fe nanoparticles.[42] In these studies, the core-shell fabrication methods take place in organic solutions, as these are typically the solvents that are used to generate the cobalt nanoparticle in the first place.

The stability of the core-shell nanoparticles is still contested, as recently pointed out by Ravel *et al.*[35] X-ray absorption spectroscopy (XAS) studies detected evidence of oxidation due to discontinuous Au coatings around Fe nanoparticles fabricated using the reverse micelle synthesis approach. They speculate that this is an unintended consequence of the reverse micelle methodology.

In this paper, a displacement method is presented to generate copper shells surrounding Co nanoparticles in aqueous solution at room temperature. To the authors' knowledge, it is the first demonstration of a copper shell around an iron-group element nanoparticle. Additionally, the shell synthesis is carried out while the nanoparticles are exposed to air. The exchange reaction takes place in an acid copper-citrate electrolyte[43] where cobalt oxides are not stable.[44] The process eliminates the need for strict N_2 control after the nanoparticle synthesis. Cobalt oxides can straightforwardly be distinguished with synchrotron X-ray absorption near-edge structure (XANES) techniques, and data showing the absence of oxides in the resulting Co-Cu nanoparticles are presented here. In addition, Cu and Co should have limited miscibility, as suggested by thermodynamic data,[45] which supports the motive for the Cu shell. However, nonequilibrium phases of CoCu can occur, as found in electrodeposited CoCu alloys.[46-48]

Experimental

Synthesis of cobalt nanoparticles.—A wet chemical approach using a sulfobetaine, dodecyldimethyl (3-sulfopropyl) ammonium hydroxide (SB-12, 98%) as a stabilizer[49] was used to synthesize the cobalt nanoparticles in tetrahydrofuran (THF). A mixture of 100 mL SB-12 (0.015 M) in THF and 15 mL of a superhydride-THF solution (1 M lithium hydrotriethyl borate in THF solvent) was added dropwise to a solution containing 100 mL $CoCl_2$ (0.0285 M) in THF solution within half an hour under ultrasonication and in an N_2 environment. The ultrasonication was continued for an additional hour, and the reaction was then quenched by adding ethanol. The solution was left undisturbed overnight and the cobalt nanoparticles precipitated by sedimentation. The cobalt nanoparticles were then washed thoroughly with THF and dried under vacuum. The confirmation of the surfactant remaining on the nanoparticles was verified by differential scanning calorimetry-thermographic analysis (TA Instruments, SDT 2960).

Displacement formation of copper shell.—The cobalt nanoparticles were added to a copper-citrate electrolyte, containing 0.25 M $CuSO_4\ 5H_2O$, 0.3 M $C_6H_5Na_3O_7\ 2H_2O$, at a pH of 4.0. The reactants were agitated ultrasonically for 1 h under atmospheric conditions. The particles were removed from the electrolyte by precipitation and washed thoroughly with deionized water. The particles were then filtered and dried under nitrogen flow.

Characterization.—Nanoparticles were characterized by transmission electron microscopy (TEM, JEOL 2010), magnetization measurements, and XAS. Samples for TEM were prepared by dropping and evaporating ethanol solutions of Co and aqueous Co-Cu core-shell particles on a carbon-coated copper and gold grid, respectively. Magnetic studies were carried out using a Quantum Design MPMS-5S superconducting quantum interference device magnetometer. The magnetization temperature dependence was measured in an applied magnetic field of 100 G between 4 and 300 K using zero-field-cooled (ZFC) and field-cooling (FC) procedures. The field

* Electrochemical Society Student Member.
** Electrochemical Society Active Member.
z E-mail: podlaha@che.lsu.edu

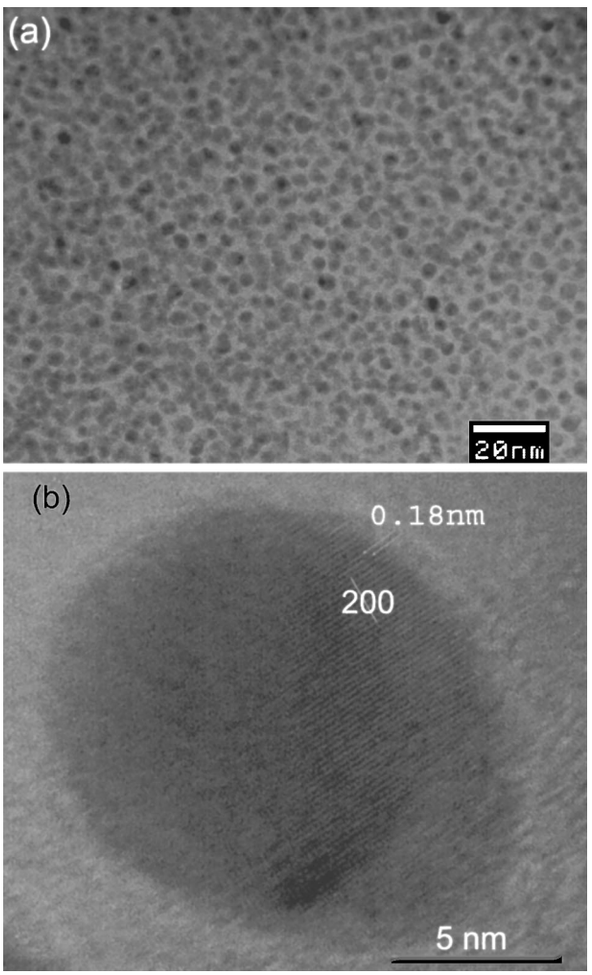

Figure 1. TEM images of Co-Cu nanoparticles at (a) low and (b) high resolution, showing a 0.175 nm Cu lattice spacing.

dependence of magnetization was measured at 10 and 300 K. The Co-Cu core-shell nanoparticle and Co nanoparticle samples for magnetic studies were placed in gelatin capsules in powder form, under atmospheric conditions and in a glove box, respectively, before being inserted in the sample space of the magnetometer.

The XAS experiments were performed at the XMP double crystal monochromator beamline at port 5A of the Center for Advanced Microstructures and Devices synchrotron radiation source at Louisiana State University. The storage ring was operated at an electron energy of 1.3 GeV. The experiments were performed in standard transmission mode using ionization chambers filled with air at 1 atm pressure. The Lemonier-type monochromator was equipped with Si(311) crystals, and the photon energy was calibrated relative to the absorption spectrum of a standard 7.5 μM Co foil, setting the first inflection point at an energy of 7709 eV. XANES spectra were collected in the −100 to +250 eV range relative to the Co K edge, with approximate step sizes of 0.5 eV and 1 s integration time per period. Samples for XAS measurement were prepared by spreading a thin layer of the dried particles uniformly over Kapton tape in air for the Co-Cu nanoparticles and in a glove box for the Co nanoparticles.

The electrochemical reaction rates were characterized on a rotating disk electrode (RDE) using linear sweep voltammetry (Solartron SI1287 and 1255B). The electrode disk area was 0.283 cm^2, and the rotation rate was 400 rpm. A Cu disk working electrode was used to characterize the kinetic range of the Cu reduction reaction, and a Co disk working electrode was used to characterize the anodization of

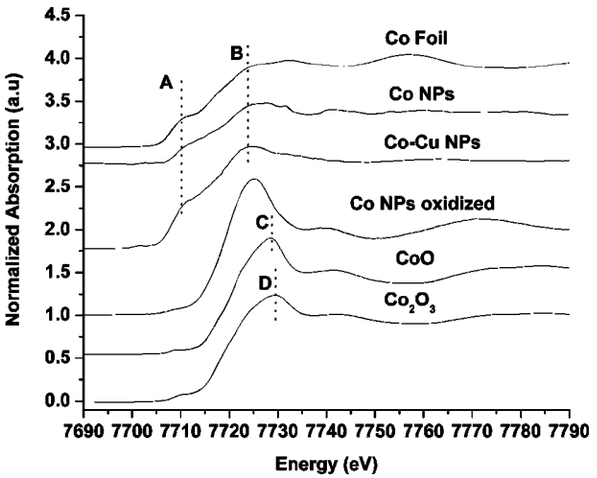

Figure 2. Co K edge XANES spectra of a hcp cobalt foil, cobalt nanoparticles, Co-Cu nanoparticles, Co nanoparticle oxidized in air, and a CoO and Co_2O_3 reference. Lines A, B, C, and D are the zero valence Co pre-edge, Co white line, and CoO and Co_2O_3 white lines, respectively.

Co. The counter electrode was Cu during the Cu reduction study and Pt during the Co anodization case. The applied sweep rate was 5 mV/s.

Results and Discussion

Figure 1 shows TEM images of the Co-Cu nanoparticles. As shown in Fig. 1a, the particles are discretely dispersed, having a mean diam of 3.2 nm with a standard deviation of 0.6 nm. The fringes shown in Fig. 1b have an interplanar distance of 0.18 nm. The lattice parameters of Cu and Co are 0.3615 and 0.3544 nm, respectively. Assuming a cubic structure, the measured d-spacing corresponds to a (2 0 0) face-centered cubic plane, consistent with a Cu shell. But due to the small difference in the lattice constants between Co and Cu, the measured d-spacing could also represent Co. A contrast difference, which can arise from the lattice fragments having different orientations with respect to the electron beam, has been reported as a distinguishing criterion for a core-shell structure.[50-52] However, here the very small difference in atomic number *Z* does not make the core-shell structure distinguishable by TEM. An estimate of the Cu shell size was calculated to be 0.82 nm based on the following: average composition of the Cu content in the nanoparticles was 87.5 wt %, determined by atomic adsorption, assuming spherical particles and bulk densities. The subsequent loss in the Co radius is thus 0.78 nm.

XAS was used to verify, indirectly, the Co core protected by the Cu shell. Figure 2 shows the XANES Co K edge spectra of a standard hexagonal close-packed (hcp) Co foil, Co nanoparticles prepared in a glove box with nitrogen protection, Co-Cu nanoparticles exposed to air, Co nanoparticles exposed to air, and two cobalt oxide standards. The XANES spectrum of Co in the Co-Cu core-shell nanoparticle differs from the cobalt oxide spectra and is similar to the spectra of the air-protected Co nanoparticle and standard Co foil. The Co XANES spectrum of the Co-Cu sample exhibits a pre-edge feature at approximately 7709 eV (line A), assigned to an electron transition from 1s to a hybridized p-d orbital, and a white line at about 7724 eV (line B). The position of the absorption edge in the Co-Cu spectrum, as well as the intensity, and the energy location of the maximum white line closely resemble those of the Co nanoparticles and the standard hcp Co foil. The chemical shift of the absorption edge to higher energies (7728 eV), lower pre-edge intensity, and higher white line (lines C and D) evident in the spectra of CoO and Co_2O_3 were not observed in the Co-Cu sample or the N_2-protected Co nanoparticle sample. Numerous literature studies have shown that when Co nanoparticles are exposed to air they readily

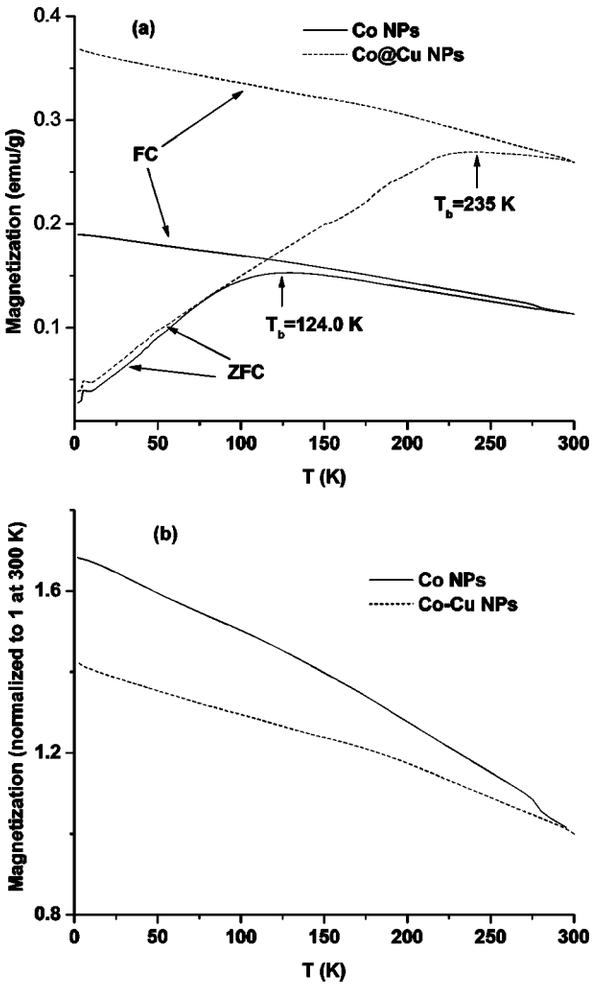

Figure 3. (a) ZFC and FC magnetization of Co and Co-Cu core-shell nanoparticles with an applied magnetic field of 100 Oe and (b) FC magnetization of Co and Co-Cu core-shell nanoparticles normalized at 300 K.

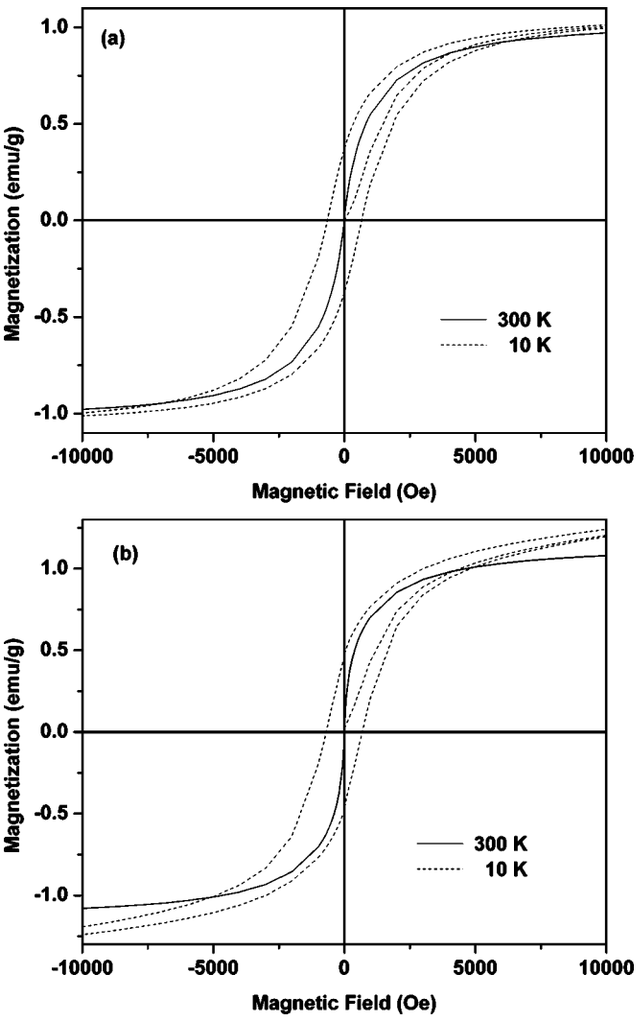

Figure 4. Hysteresis loops for Co and Co-Cu nanoparticles at 10 and 300 K.

oxidize,[2,11,13,53,54] and this is confirmed as well in the XANES spectra in Figure 2. Thus, the XANES experiments prove that the Cu shell has effectively protected the Co nanoparticle from oxidation.

The temperature dependence of the magnetization is shown in Fig. 3. The blocking temperature (T_b), the transition temperature between the ferromagnetic and the superparamagnetic state, is determined from the maximum in the ZFC measurements. T_b is increased for the Co-Cu core-shell nanoparticles (235 K) compared with the precursor Co nanoparticles (124 K). An increase of the blocking temperature due to antiferromagnetic exchange coupling has also been reported for compacted Co-CoO core-shell nanoparticles[55] and for Co nanoparticles dispersed in a CoO matrix.[34] In our study, the data suggest that there is little or no CoO formed, so the higher blocking temperature may be due to an increase in dipole interactions between the Co particles, as observed in Co clusters.[56] In the FC curve, the magnetization decays uniformly as the temperature increases in both of these nanoparticle cases and can be used to evaluate particle interaction.[57-59] The normalized FC magnetization curves (Fig. 3b) show a difference in slope between the Co and the Co-Cu core-shell nanoparticles. The slope of the Co-Cu nanoparticles curve is lower than that of the Co nanoparticles. A smaller slope in the FC magnetization of the Co-Cu core-shell nanoparticle indicates a stronger interparticle interaction compared to Co nanoparticles, consistent with literature studies[58] and the observed increase in the blocking temperature here.

The field dependence of magnetization is shown in Fig. 4a and b for Co and Co-Cu core-shell nanoparticles, respectively, and the magnetic parameters are summarized in Table I. At 10 K, well below the blocking temperature, a nonzero coercivity and remnant magnetization are expected; whereas, near room temperature (*i.e.*, above the blocking temperature), coercivity and remnant magnetization are zero, indicative of the superparamagnetic state. The observed coercivity of the Co-Cu core-shell nanoparticle (−697 Oe) is slightly larger than that of the Co precursor (−656 Oe) at 10 K. The remnant magnetization increased from 0.37 emu/g for the Co nanoparticle to 0.47 emu/g for the Co-Cu core-shell nanoparticle at 10 K, where the mass used is the total sample mass. The Co mass content in the cobalt paste sample and in the Co-Cu sample is 8.4 and 4.0%, respectively. The majority of the mass in the samples consists of

Table I. Magnetic properties of Co and Co-Cu nanoparticles (NPs).

Sample	T (K)	H_c (Oe)	M_r (emu/g)	M_s (emu/g)	M_r/M_s
Co NPs	10	−656.0	0.37	1.01	0.37
	300	0	0	1.05	0
Co-Cu NPs	10	−697.0	0.47	1.53	0.31
	300	0	0	1.06	0

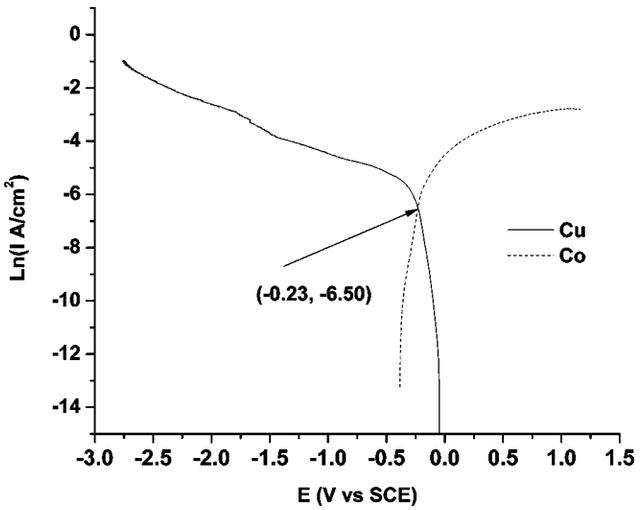

Figure 5. Evans diagram for cobalt anodization and copper reduction on RDE at 400 rpm.

surfactant. The enhanced magnetization is also reflected in the temperature dependence of the magnetization curve, as shown in Fig. 3. Thus, the magnetization is slightly higher for the Co-Cu nanoparticles than for the Co nanoparticles, based on a per unit mass of elemental cobalt.

The displacement reaction rate was estimated from an Evans diagram, shown in Fig. 5. The rotation rate was arbitrarily selected so that it was large enough to capture the kinetic regime of both the bulk cobalt anodization in a copper-free electrolyte and the copper reduction from a copper electrolyte. The mixed potential corrosion current thus represents an upper limit on the reaction rate. Mass-transport limitations would lower this value. Due to the ultrasonic stirring used during the shell fabrication, a kinetic-controlled process is expected, rather than a diffusion-controlled process. The crossing point $(-0.23, -6.50)$ of the anodic and cathodic branches of these two reactions determines the displacement potential of -0.23 V *vs.* a saturated calomel electrode and the corresponding current density of $(e^{-6.5}) = 0.0015$ A/cm^2. Therefore, using an average particle diameter from the TEM micrographs of 3.2 nm, with an average surface area of 3.22×10^{-13} cm^2, results in an average reaction rate of 2.51×10^{-21} mol/s/particle.

In the absence of Cu(II) ions, the Co nanoparticle is expected to be anodized by protons in the electrolyte, leading to a complete loss of the Co solid nanoparticle to Co(II) ions. The fact that Co nanoparticles are preserved in the aqueous acidic environment is another confirmation of the Cu shell formation.

Conclusion

A nanoparticle core-shell structure was fabricated by a displacement reaction between the Co core and Cu(II) ions in a typical aqueous electrolyte. XANES results are consistent with the encapsulation of the Co nanoparticles by Cu without any significant cobalt oxide. The magnetization of the Co nanoparticle was retained when it was protected by the Cu shell and exposed to air. An increase in the blocking temperature was observed up to 235 K for the core-shell nanoparticles, compared with 124 K for Co nanoparticles. An estimate of the displacement rate of cobalt atoms with copper ions was calculated to be 2.51×10^{-21} mol/s/particle.

Acknowledgments

This project was supported by NSF-EPSCoR [(2001-04)RII-03], NSF CAREER (ECS-9984775), and the Defense Advanced Research Projects Agency (MDA 972-63-C-0100). The authors kindly thank Dr. J. Jiang and Dr. J. Zhang at Louisiana State University for help with the TEM instrument operation and the electrochemical experiments, respectively, and Carol A. Carter, Ann Arbor, Michigan, for the atomic adsorption analysis.

Louisiana State University assisted in meeting the publication costs of this article.

References

1. J. P. Chen, C. M. Sorensen, K. J. Klabunde, and G. C. Hadjipanayis, *J. Appl. Phys.*, **76**, 6316 (1994).
2. H. Bonnemann, W. Brijoux, R. Brinkmann, N. Matoussevitch, N. Waldofner, N. Palina, and H. Modrow, *Inorg. Chim. Acta*, **350**, 617 (2003).
3. C. B. Murray, S. Sun, H. Doyle, and T. Betley, *MRS Bull.*, **26**, 985 (2001).
4. V. F. Puntes, K. M. Krishnan, and A. P. Alivisatos, *Science*, **291**, 2115 (2001).
5. O. Kitakami, H. Sato, Y. Shimada, F. Sato, and M. Tanaka, *Phys. Rev. B*, **56**, 13849 (1997).
6. J. P. Chen, K. M. Lee, C. M. Sorensen, K. J. Klabunde, and G. C. Hadjipanayis, *J. Appl. Phys.*, **75**, 5876 (1994).
7. C. Petit, A. Taleb, and M. P. Pileni, *J. Phys. Chem. B*, **103**, 1805 (1999).
8. X. M. Lin, C. M. Sorensen, K. J. Klabunde, and G. C. Hadjipanayis, *Langmuir*, **14**, 7140 (1998).
9. J. Osuna, D. C. Dominique, C. Amiens, B. Chaudret, E. Snoeck, M. Respaud, J. Broto, and A. Fert, *J. Phys. Chem.*, **100**, 14571 (1996).
10. S. Ram, *Mater. Sci. Eng., A*, **304-306**, 923 (2001).
11. S. H. Sun and C. B. Murray, *J. Appl. Phys.*, **85**, 4325 (1999).
12. V. F. Puntes, K. Krishnan, and A. P. Alivisatos, *Top. Catal.*, **19**, 145 (2002).
13. D. P. Dinega and M. G. Bawendi, *Angew. Chem., Int. Ed. Engl.*, **38**, 1788 (1999).
14. Y. W. Zhao, R. K. Zheng, X. X. Zhang, and J. Q. Xiao, *IEEE Trans. Magn.*, **39**, 2764 (2003).
15. S. Gangopadhyay, G. C. Hadjipanayis, B. Dale, C. M. Sorensen, K. J. Klabunde, V. Papaefthymiou, and A. Kostikas, *Phys. Rev. B*, **45**, 9778 (1992).
16. D. Farrell, S. A. Majetich, and J. P. Wilcoxon, *J. Phys. Chem. B*, **107**, 11022 (2003).
17. S. N. Khanna and S. Linderoth, *Phys. Rev. Lett.*, **67**, 742 (1991).
18. S. E. Apsel, J. W. Emmert, J. Deng, and L. A. Bloomfield, *Phys. Rev. Lett.*, **76**, 1441 (1996).
19. D. L. LesliePelecky and R. D. Rieke, *Chem. Mater.*, **8**, 1770 (1996).
20. L. Yiping, G. C. Hadjipanayis, C. M. Sorensen, and K. J. Klabunde, *J. Appl. Phys.*, **75**, 5885 (1994).
21. S. Sun, C. B. Murray, D. Weller, L. Folks, and A. Moser, *Science*, **287**, 1989 (2000).
22. S. Wang, S. S. Kang, D. E. Nikles, J. W. Harrell, and X. W. Wu, *J. Magn. Magn. Mater.*, **266**, 49 (2003).
23. M. Tanase, N. T. Nuhfer, D. E. Laughlin, T. J. Klemmer, C. Liu, N. Shukla, X. Wu, and D. Weller, *J. Magn. Magn. Mater.*, **266**, 215 (2003).
24. Y. Xu, Z. G. Sun, Y. Qiang, and D. J. Sellmyer, *J. Magn. Magn. Mater.*, **266**, 164 (2003).
25. T. Iwaki, Y. Kakihara, T. Toda, M. Abdullah, and K. Okuyama, *J. Appl. Phys.*, **94**, 6807 (2003).
26. H. Zeng, S. Sun, R. L. Sandstrom, and C. B. Murray, *J. Magn. Magn. Mater.*, **266**, 227 (2003).
27. T. O. Ely, C. Pan, C. Amiens, B. Chaudret, F. Dassenoy, P. Lecante, M. J. Casanove, A. Mosset, M. Respaud, and J. M. Broto, *J. Phys. Chem. B*, **104**, 695 (2000).
28. K. E. Elkins, T. S. Vedantam, J. P. Liu, H. Zeng, S. Sun, Y. Ding, and Z. L. Wang, *Nano Lett.*, **3**, 1647 (2003).
29. A. Kumbhar, L. Spinu, F. Agnoli, K. Wang, W. Zhou, and C. J. O'Connor, *IEEE Trans. Magn.*, **37**, 2216 (2001).
30. E. V. Shevchenko, D. V. Talapin, A. L. Rogach, A. Kornowski, M. Haase, and H. Weller, *J. Am. Chem. Soc.*, **124**, 11480 (2002).
31. Z. H. Wang, C. J. Choi, J. C. Kim, B. K. Kim, and Z. D. Zhang, *Mater. Lett.*, **57**, 3560 (2003).
32. N. Chakroune, G. Viau, C. Ricolleau, F. Fievet-Vincent, and F. Fievet, *J. Mater. Chem.*, **13**, 312 (2003).
33. R. D. Zysler, H. Romero, C. A. Ramos, E. De Biasi, and D. Fiorani, *J. Magn. Magn. Mater.*, **266**, 233 (2003).
34. V. Skumryev, S. Stoyanov, Y. Zhang, G. Hadjipandyis, D. Givord, and J. Nogues, *Nature (London)*, **423**, 850 (2003).
35. B. Ravel, E. E. Carpenter, and V. G. Harris, *J. Appl. Phys.*, **91**, 8195 (2002).
36. W. L. Zhou, E. E. Carpenter, J. Lin, A. Kumbhar, J. Sims, and C. J. O'Connor, *Eur. Phys. J. D*, **16**, 289 (2001).
37. M. Chen, S. Yamamuro, D. Farrell, and S. A. Majetich, *J. Appl. Phys.*, **93**, 7551 (2003).
38. J. Lin, W. Zhou, A. Kumbhar, J. Wiemann, J. Fang, E. E. Carpenter, and C. J. O'Connor, *J. Solid State Chem.*, **159**, 26 (2001).
39. E. E. Carpenter, A. Kumbhar, J. A. Wiemann, H. Srikanth, J. Wiggins, W. Zhou, and C. J. O'Connor, *Mater. Sci. Eng., A*, **286**, 81 (2000).
40. J.-I. Park and J. Cheon, *J. Am. Chem. Soc.*, **123**, 5743 (2001).
41. A. J. Garcia-Bastida, R. D. Sanchez, J. Garcia-Otero, J. Rivas, A. Gonzalez-Penedo, J. Solla, and M. A. Lopez-Quintela, *Mater. Sci. Forum*, **269**, 919 (1998).
42. D. A. Fleming, M. Napolitano, and M. E. Williams, *Mater. Res. Soc. Symp. Proc.*, **746**, 207 (2003).
43. E. J. Podlaha, *Nano Lett.*, **1**, 413 (2001).
44. M. Pourbaix, *Atlas of Electrochemical Equilibria in Aqueous Solutions*, Cebelcor, Houston, TX (1974).

45. *Binary Alloy Phase Diagrams*, 2nd ed., T. B. Massalski, Editor, ASM International, Materials Park, OH (1990).
46. T. Cohen-Hyams, W. D. Kaplan, D. Aurbach, Y. S. Cohen, and J. Yahalom, *J. Electrochem. Soc.*, **150**, C28 (2003).
47. Y. Ueda, T. Houga, H. Zaman, and A. Yamada, *J. Solid State Chem.*, **147**, 274 (1999).
48. E. Gomez, A. Labarta, A. Llorente, and E. Valles, *J. Electroanal. Chem.*, **517**, 63 (2001).
49. H. Bonnemann, W. Brijoux, and T. Joussen, *Angew. Chem., Int. Ed. Engl.*, **29**, 273 (1990).
50. C. B. Murray, S. H. Sun, W. Gaschler, H. Doyle, T. A. Betley, and C. R. Kagan, *IBM J. Res. Dev.*, **45**, 47 (2001).
51. X. Teng and H. Yang, *J. Am. Chem. Soc.*, **125**, 14559 (2003).
52. Y. Mizukoshi, T. Fujimoto, Y. Nagata, R. Oshima, and Y. Maeda, *J. Phys. Chem. B*, **104**, 6028 (2000).
53. D. L. Peng, K. Sumiyama, T. J. Konno, T. Hihara, and S. Yamamuro, *Phys. Rev. B*, **60**, 2093 (1999).
54. D. L. Peng, K. Sumiyama, T. Hihara, S. Yamamuro, and T. J. Konno, *Phys. Rev. B*, **61**, 3103 (2000).
55. M. Z. Wu, Y. D. Zhang, S. Hui, T. D. Xiao, S. H. Ge, W. A. Hines, J. I. Budnick, and M. J. Yacaman, *J. Appl. Phys.*, **92**, 6809 (2002).
56. F. Luis, F. Petroff, J. M. Torres, L. M. Garcia, J. Bartolome, J. Carrey, and A. Vaures, *Phys. Rev. Lett.*, **88**, 217205 (2002).
57. A. F. Gross, M. R. Diehl, K. C. Beverly, E. K. Richman, and S. H. Tolbert, *J. Phys. Chem. B*, **107**, 5475 (2003).
58. M. Hanson, C. Johansson, M. S. Pedersen, and S. Morup, *J. Phys.: Condens. Matter*, **7**, 9269 (1995).
59. R. W. Chantrell, N. S. Walmsley, J. Gore, and M. Maylin, *J. Appl. Phys.*, **85**, 4340 (1999).